Journal of Nuclear Materials 385 (2009) 319–324

Contents lists available at ScienceDirect

Journal of Nuclear Materials

journal homepage: www.elsevier.com/locate/jnucmat

Study of atomic clusters in neutron irradiated reactor pressure vessel surveillance samples by extended X-ray absorption fine structure spectroscopy

S. Cammelli [a,b,*], C. Degueldre [a], G. Kuri [a], J. Bertsch [a], D. Lützenkirchen-Hecht [b], R. Frahm [b]

[a] LWV, NES, Paul Scherrer Institute, 5232 Villigen PSI, Switzerland
[b] Fachbereich C - Physik, Bergische Universität Wuppertal, Gauß-Str. 20, 42097 Wuppertal, Germany

ARTICLE INFO

PACS:
28.41.Qb
28.50.Hw
61.05.cj

ABSTRACT

Copper and nickel impurities in nuclear reactor pressure vessel (RPV) steel can form nano-clusters, which have a strong impact on the ductile–brittle transition temperature of the material. Thus, for control purposes and simulation of long irradiation times, surveillance samples are submitted to enhanced neutron irradiation. In this work, surveillance samples from a Swiss nuclear power plant were investigated by extended X-ray absorption fine structure spectroscopy (EXAFS). The density of Cu and Ni atoms determined in the first and second shells around the absorber is affected by the irradiation and temperature. The comparison of the EXAFS data at Cu and Ni K-edges shows that these elements reside in arrangements similar to bcc Fe. However, the EXAFS analysis reveals local irradiation damage in the form of vacancy fractions, which can be determined with a precision of ~5%. There are indications that the formation of Cu and Ni clusters differs significantly.

1. Introduction

The reactor pressure vessel (RPV) is one of the most important barriers between the core and the environment of a nuclear reactor; its integrity must be guaranteed at all times. The degradation of the RPV is an important issue as it can lead to plant lifetime limitations.

RPV steels are iron alloys and the degradation of the mechanical properties is due to a shift of the ductile to brittle transition temperature. The key embrittlement mechanisms is related to the formation of a high number density ($>10^{23}$ m^{-3}) of ultra-fine precipitates resulting from the irradiation and diffusion processes in the damaged matrix lattice [1–5]. The contribution of the various alloying elements and impurities (e.g. Cu, Ni, Mn, P, Si etc.) to irradiation hardening and embrittlement have been studied intensively [6–8]. Besides neutron irradiation also thermal influences affect the embrittlement of the vessel steel [5].

Copper plays a major role for the embrittlement process and consequently it has been studied extensively [9,10]. Copper is almost insoluble in iron even at high temperatures, and therefore small amounts of copper are enough to produce small precipitates.

Most of the XAFS studies were performed on binary [10], ternary or quaternary [11,12] alloys composed mostly by Fe, Cu, Ni and Mn. Important studies were also performed using atom probe tomography (APT) on a binary alloy [9,13], ternary alloy [14] and RPV steel [5,15,16]. In the literature two main aspects were discussed for iron alloys with low copper content smaller than about 0.2 at.%. First of all, Cu precipitates were only found if the radiation is able to produce a vacancy density which is large enough to facilitate the migration of atoms [9], and second, the profile of the precipitates shows that the element with the highest concentration in the clusters is Cu [5]. This effect is very pronounced mainly due to the very low solubility of Cu in the iron matrix which is below 0.1 at.% at ~775 K [17,18].

Extended X-ray absorption fine structure spectroscopy (EXAFS) has been used here as analyzing tool because it is an element specific and non-destructive method. EXAFS explores the modulations of the X-ray absorption coefficient above the absorption edge of an element of interest and is caused by the scattering of the ejected photoelectrons from neighbouring atoms. EXAFS can provide structural information up to ~6 Å around the absorber atom at room temperature, and even further at low temperatures. The 1st and 2nd nearest neighbour numbers, the elements that compose these shells and the interatomic distances can be investigated with a high accuracy.

The main goal of this paper is to study the atomic environment of Cu and Ni in RPV steel. It has been previously shown that Cu is the main element in the nano-clusters [9]. Nickel may also be present in the clusters but its role is not completely clear. It is still important to understand how the number and the type of atoms in the first and second shell around copper and nickel changes with neutron irradiation, and how their environment, especially vacancies, is modified by the irradiation and temperature influences.

* Corresponding author. Address: LWV, NES, Paul Scherrer Institute, 5232 Villigen PSI, Switzerland. Tel.: +41 56 310 5439.
E-mail address: Sebastiano.cammelli@psi.ch (S. Cammelli).

0022-3115/$ - see front matter © 2008 Published by Elsevier B.V.
doi:10.1016/j.jnucmat.2008.12.019

Finally it has to be pointed out that this is the first EXAFS study with RPV steel provided by a power plant after irradiation.

2. Theory

The theory of EXAFS has been discussed in several studies [19,20]. RPV steels include several elements, here denominated M_1, M_2,... M_n dissolved in the matrix of M_0. A heat treatment and neutron irradiation can affect significantly the atomic environment of each element in the matrix and these changes can be investigated in detail by an element specific technique as EXAFS. Because of the low degree of solubility of some elements, such as Cu and Ni, in the matrix the sample alloy cannot be considered as homogeneous solution.

2.1. Solid solution

The model applied in our EXAFS data analysis describes a simplified system. The matrix utilized for the model is considered to be composed by only two elements M_0 and M_1. These two elements are weighted with two parameters: x and y where x represents the fraction of M_0 in the first shell and y in the second. Consequently $(1-x)$ and $(1-y)$ represents the fraction of M_1 in the first and second shells, respectively. Therefore it follows:

$$N_{M_0} = N\left[\frac{8}{14}x + \frac{6}{14}y\right]$$

$$N_{M_1} = N\left[\frac{8}{14}(1-x) + \frac{6}{14}(1-y)\right], \quad (1)$$

where N is the experimental sum of the next neighbours number in the two first shells in the bcc lattice. The only boundary conditions are:

$$0 \leqslant N_{M_0} \leqslant 14 \quad \text{and} \quad 0 \leqslant N_{M_1} \leqslant 14 \quad (2)$$

x and y expected to be $0 \leqslant x \leqslant 1$ and $0 \leqslant y \leqslant 1$. However, the first and the second shells convolute in the first main peak of the Fourier Transform (FT) of the EXAFS signal and thus, they can not be considered separately. The high correlation of the two shells implies a high correlation of all the variables that refer to these shells.

Some theoretical limitations prevent EXAFS spectroscopy to recognize elements belonging to the environment with a difference of atomic number smaller than two (e.g. Cu and Ni); these elements behave as almost equivalent backscatters. In this case it is not possible to separate them, identifying finally individual contribution to the EXAFS signal. This is true only if the Cu and Ni atoms behave in the same way. Therefore the notation $N_{M_1M_2}$ will be used to identify the numbers of atoms M_1 plus the number of M_2 in the 1st and 2nd shells.

3. Experimental

3.1. Samples

The material investigated is an iron based ferritic steel designated here as KKG. The chemical composition of the material is given in Table 1. The samples were provided by the nuclear power plant of Gösgen (Däniken, Switzerland).

An unirradiated reference sample, here denominated REF, and three differently irradiated samples have been obtained. All these samples had been submitted to the same pre-treatments (e.g. ~10 h at ~880 K). For irradiation, the surveillance samples were positioned close to the reactor core. The samples, inside capsules, were placed at 2 m from the axial core centre and roughly 25 cm below the mid core level. Because of the shorter distance to the core, the fluence is enhanced by a certain factor, reducing time for obtaining representative irradiation damage. Consequently, the fluence recorded on these surveillance samples was about 12 times larger than the fluence recorded on the actual reactor pressure vessel. The samples were exposed to the same temperature as that of the reactor water, i.e. ~575 K. The three surveillance samples were irradiated for 1, 3 and 4 years; they are denominated HI1, HI3 and HI4, respectively (see Table 2).

3.2. XAFS analysis

3.2.1. Experimental

The XAFS analysis was performed at the micro-XAS beamline of the Swiss light source (SLS) synchrotron radiation facility [21]. The electron current in the storage ring was around 400 mA. The beamline uses a double crystal monochromator to select the required energy with a pair of Si (1 1 1) crystals. The incident X-ray intensity was measured by means of an ultra-thin silicon based diode. A 32-elements Ge solid state fluorescence detector was applied to record the XAFS spectra in fluorescence mode. Cu and Ni K-edges were investigated here. The specimens were held at room temperature. As it was not required to use micro-focussed beam spots, experiments were conducted with a spot size of $250 \times 250\ \mu m^2$. The detector was placed perpendicular to the beam in the storage ring orbit plane. Several spectra (>4) were collected for each K-edge and for each sample to obtain better photon counting statistics.

Additionally, the REF sample was also analyzed at the XAS beamline at ANKA at the Forschungszentrum Karlsruhe (FZK) [22]. The average current in the storage ring was around 140 mA. This analysis was performed in a cryostat at 15 K. A five element Ge solid state fluorescence detector was applied to record spectral data. The detector, beam and sample holder have the same geometrical configuration compared to that at the microXAS beamline.

3.2.2. Data analysis software

The data analysis was performed with the HORAE package, an EXAFS software including ATHENA, ARTEMIS [23–25]. In the data analysis the theoretical model, is adapted to the FT of the EXAFS spectra [19,20] extracted by the experimental data.

4. Results and discussion

4.1. Theoretical model hypothesis

The theoretical spectrum is calculated with feff.inp, an input file based on crystallographic assumptions. Firstly it was assumed that the steel matrix has the same crystallographic structure as pure iron which is ~97 at.% of the steel. This assumption was confirmed to be correct from the shape of the absorption edge (Figs. 1 and 2). Two different environments were used, Fe–Cu and Fe–Ni. For both, the same results were obtained and finally the environment Fe–Cu was chosen with which all the data were analyzed. As previously

Table 1
Elemental composition of the KKG steel material. Indicated in bold are the absorber elements investigated in this study. The iron fraction is the balance.

Element	C	Al	Si	P	S	V	Cr	Mn	**Ni**	**Cu**	Mo
Fraction (at.%)	0.78	0.04	0.26	0.01	0.013	0.01	0.43	0.84	**0.89**	**0.08**	0.20

Table 2
Neutron fluences and temperature of the samples. The actual reactor pressure vessel was submitted to an average neutron flux of 6.75×10^{18} cm^{-2} a^{-1} ($E \geqslant 0.821$ MeV); the surveillance samples were submitted to a neutron flux 12 times larger.

KKG samples	Irradiation, n fluence φ (cm^{-2})	Thermal conditions	
		T (K)	t (a)
REF	0	~300	10
HI1	4.75×10^{18}	575	1
HI3	1.09×10^{19}	575	3
HI4	2.60×10^{19}	575	4

noted it is not possible to differentiate between Cu and Ni. Consequently $N_{Cu,Ni}$ is the sum of Cu and Ni atoms in the two first shells.

4.2. EXAFS: Cu K-edge

Experimental EXAFS spectra, their FT and the results obtained from the detailed analysis at the Cu K-edge are shown in Figs. 3 and 4 and Table 3. The analysis of the reference sample was (independently) performed on the two sets of experimental data collected at 15 K (measured at ANKA) and at room temperature (measured at SLS). Only data collected under the same experimental conditions can be directly compared because of the thermal expansion of the lattice and the temperature dependence of the lattice vibrations. Unfortunately, it was not possible to investigate the irradiated samples at 15 K, which would have been favourable because the EXAFS oscillations are more pronounced due to the reduced amplitude of the lattice vibrations at low temperatures.

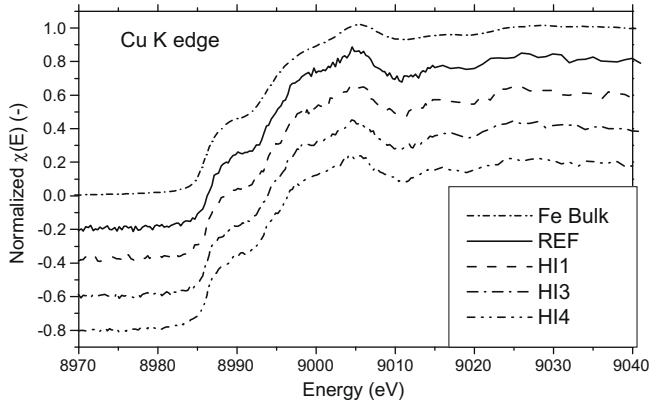

Fig. 1. The spectra of Fe bulk (shifted at the Cu absorption energy), of REF, HI1, HI3 and HI4 at the Cu K-edge.

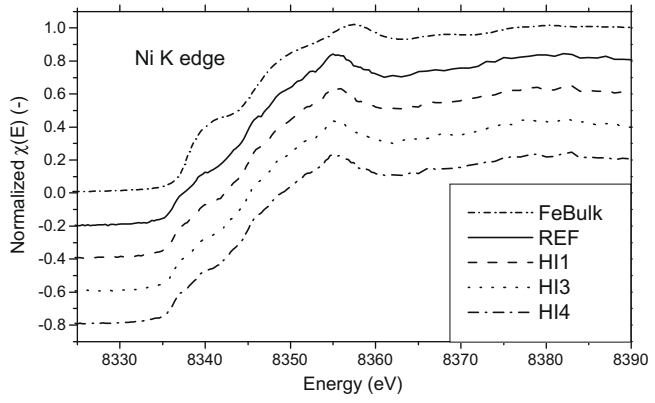

Fig. 2. The spectra of Fe bulk (shifted at the Ni absorption energy), of REF, HI1, HI3 and HI4 at the Ni K-edge.

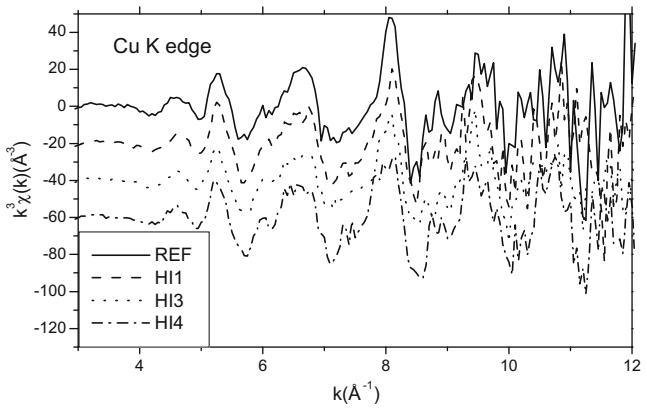

Fig. 3. The EXAFS spectra $\chi(k)$ of the sample REF, HI1, HI3 and HI4 at the Cu K-edge. $\chi(k)*k^3$ is used to increase the contribution at large k.

As major results, however, the experiments at cryogenic temperature and at room temperature reveal the same amount of Cu and Ni atoms in the first and second shells. Consequently the RT reference analysis was performed setting the x, y values to those values which were obtained at 15 K. The data analysis was performed on the Fourier Transform of the EXAFS signal (Figs. 3 and 4). The EXAFS spectra were firstly increased by a factor k^3 to point out the contribution at high k and then filtered by a Hanning window $W(k)$ with 4 Å^{-1} < k < 11 Å^{-1}, dk = 0.5 Å^{-1} (Figs. 3 and 4).

As can be seen in Fig. 4, the overall shape of the FT data is unchanged but reduced in amplitude after irradiation of the RPV steels. Due to the limited data quality, investigations of the 3rd shell and beyond were not performed here because the results would be affected by large uncertainties. However, the results determined by a detailed analysis of the two first shells have reasonable error limits. In Table 3, the most important parameters obtained from the detailed data analysis are compiled. Δr is the difference in the atomic distances for the 1st and 2nd shell atoms, determined by the fit and the model structure which was the basis for the ab-initio calculation of the EXAFS by FEFF. The Debye Waller factor $e^{-2k^2\sigma^2}$ is a function of the mean square relative displacement σ^2, the measure of the variation around the equilibrium position due to thermal and static disorders. σ^2 for the first shell is lower than the σ^2 for the second shell. This change is due to interstitials, and to the complex composition of the samples

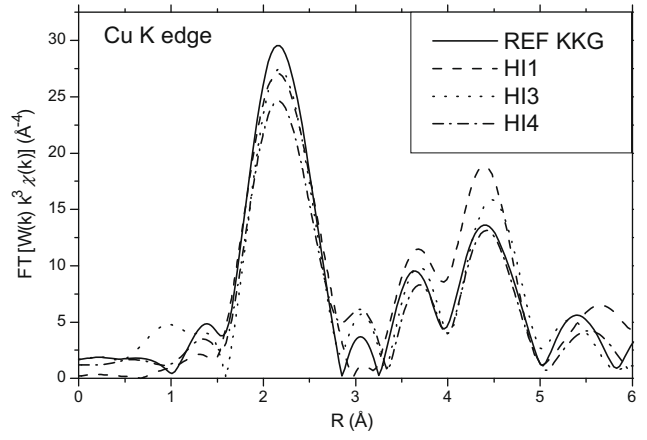

Fig. 4. The FT of REF, HI1, HI3 and HI4 at the Cu K-edge. Conditions: $W(k)$ is the Hanning function 4 Å^{-1} < k < 11 Å^{-1}, dk = 0.5 Å^{-1}.

Table 3
Comparison of the distance shift (Δr), the mean square relative displacement (σ^2), number of atoms in the first and second shell (N) and number of Cu and Ni atoms in the two first shells at the Cu K-edge ($N_{Cu,Ni}$) as determined by a fit of the measured EXAFS. The distance shift Δr is compared to the theoretical model (first shell distance: 2.482 ± 0.001 Å; second shell distance: 2.867 ± 0.001 Å for bcc Fe).

Cu K-edge	Shell	REF (15 K)	REF (RT)	HI1	HI3	HI4
Δr (Å)	1st	−0.030 ± 0.005	−0.008 ± 0.002	−0.019 ± 0.004	−0.019 ± 0.007	−0.01 ± 0.01
σ^2 (Å^2)		0.006 ± 0.001	0.003 ± 0.001	0.004 ± 0.001	0.004 ± 0.001	0.004 ± 0.001
Δr (Å)	2nd	−0.063 ± 0.002	−0.019 ± 0.009	−0.025 ± 0.008	−0.02 ± 0.01	−0.05 ± 0.01
σ^2 (Å^2)		0.002 ± 0.001	0.010 ± 0.002	0.007 ± 0.001	0.012 ± 0.002	0.011 ± 0.002
N	1st and 2nd	14.0 ± 0.1	14.0 ± 0.1	14.0 ± 0.5	13.9 ± 0.4	13.5 ± 0.4
$N_{Cu,Ni}$		1 ± 1	1 ± 1	0 ± 3	1 ± 3	5 ± 3

compared to the theoretical model applied. It has to be pointed out that σ^2 for the 1st shell is correlated to σ^2 for the 2nd shell, so the recorded disorder is common to both shells. Moreover, the comparison between the REF samples, measured at 15 K and at room temperature, has to take into account the high correlation between the first and second shell atoms. This high correlation makes any consideration on a single shell difficult without considering the other one. For instance, the σ^2 for the first shell of the REF sample at 15 K is larger than all the other first shell σ^2 measured at room temperature; this can be understood only considering the second shell σ^2 value. Considering the average between the first and second shell σ^2 an increase of the noise is observed as expected.

4.3. Ni K-edge

The EXAFS spectra experimentally determined by the X-ray absorption experiments at the Ni K-edge are shown in Fig. 5 and their FT in Fig. 6. The fit results are compiled in Table 4. These data were collected only at room temperature. Compared to the experiments at the Cu K-edge, those at the Ni K-edge are significantly facilitated by the higher Ni content of the RPV steel (i.e. 0.89 at.% Ni compared to only 0.08 at.% Cu), leading to higher count rates in the fluorescence detector and better counting statistics accordingly. Consequently the N and $N_{Cu,Ni}$ incertitude estimated by the evaluation software at Ni K-edge are smaller compared to those determined at the Cu K-edge (with the only exception of sample REF because N and $N_{Cu,Ni}$ incertitude is the same as REF measured at 15 K).

4.4. Discussion: effect of irradiation at 575 K

Four RPV surveillance samples have been analyzed in detail by EXAFS investigations, three irradiated in the reactor and one unirradiated as reference. Considering the total number of atoms in the

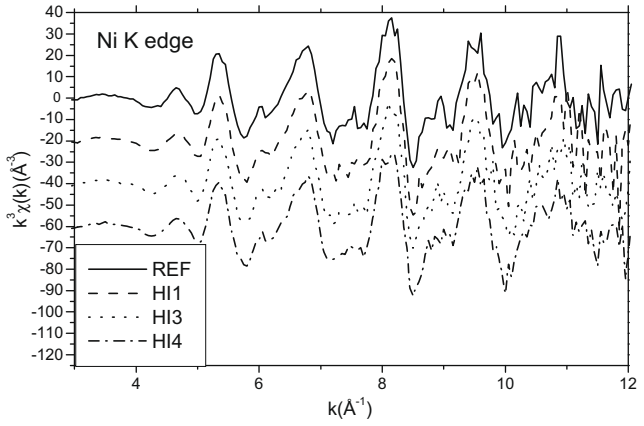

Fig. 5. The EXAFS spectra $\chi(k)$ of the sample REF, HI1, HI3 and HI4 at the Ni K-edge. $\chi(k)*k^3$ is used to increase the contribution at large k.

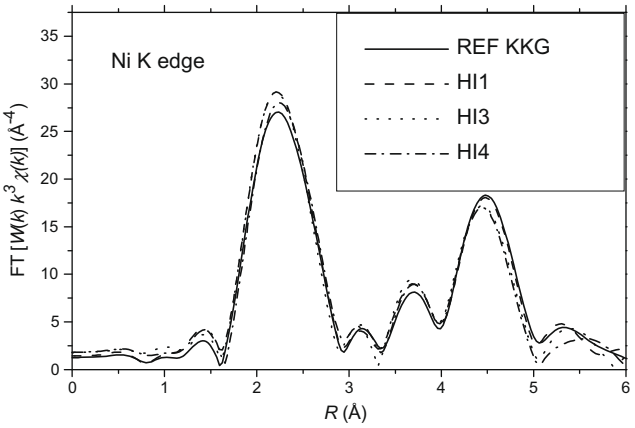

Fig. 6. The FT of REF, HI1, HI3, and HI4 at the Cu K-edge. Conditions: $W(k)$ is the Hanning function 4 Å^{-1} < k < 11 Å^{-1}, dk = 0.5 Å^{-1}.

first and second shell N, it is important to note that at the Cu K-edge N does not change significantly for the samples HI1 and HI3 (14.0 ± 0.5 and 13.9 ± 0.4, respectively) with respect to REF (14.0 ± 0.1). A significant difference was found for the sample HI4 (13.5 ± 0.4). Similar results have been obtained at the Ni K-edge with 13.9 ± 0.3 and 13.7 ± 0.4 atoms in the first and second shell around the absorber for HI1 and HI3, whereas HI4 has 13.6 ± 0.3 atoms. The decrease of the number of atoms in the first and second shell around the absorber is due to the neutron irradiation: the production of point defects is faster than the recombination of vacancies and interstitials even at the elevated irradiation temperature of 575 K. Within the accuracy of the experiments, the gained results suggest that the vacancies are similarly distributed around both the absorbers Cu and Ni as can be more clearly seen in Figs. 7. Such a result is expected because the original bcc-lattice structure of the steel is maintained after the irradiation, and both Cu- and Ni-atoms are supposed to be mainly located on regular bcc-lattice sites. Thus, the average number of point defects created in the vicinity of each atom should be similar and only depending on the applied irradiation fluence.

Considering the number of Cu and Ni atoms $N_{Cu,Ni}$ around the copper and nickel absorbers, the gained results suggest that both species do not behave in the same way (see Fig. 8). Although affected by a large error, it was found that Cu and Ni are enriched in the vicinity of the Cu atoms, while the composition of the first and second shell around Ni seems to be independent from the applied neutron irradiation. On a first glance, these findings seem to be contradicting. However, it is important here to remember that Cu and Ni atoms are not distinguishable when they both belong to the environment; their backscattering amplitudes are very similar. Assuming that copper and nickel are randomly distributed in the first and second coordination shells of both copper and nickel, the EXAFS analysis should show the similar behaviour, e.g. a decrease or an increase of $N_{Cu,Ni}$ for both edges investigated.

Table 4
Comparison of distance shift (Δr), the mean square relative displacement (σ^2), the number of atoms in the first and second shells (N) and numbers of Cu and Ni atoms in the two first shells at the Ni K-edge ($N_{Cu,Ni}$). The distance shift Δr is compared to the theoretical model (first shell distance: 2.482 ± 0.001 Å; second shell distance: 2.867 ± 0.001 Å).

Ni K-edge	Shell	REF (RT)	HI1	HI3	HI4
Δr (Å)	1st	−0.025 ± 0.004	−0.029 ± 0.003	−0.026 ± 0.002	−0.004 ± 0.003
σ^2 (Å^2)		0.007 ± 0.001	0.005 ± 0.001	0.005 ± 0.001	0.005 ± 0.001
Δr (Å)	2nd	−0.034 ± 0.003	−0.034 ± 0.004	−0.041 ± 0.006	−0.018 ± 0.004
σ^2 (Å^2)		0.004 ± 0.001	0.005 ± 0.001	0.006 ± 0.001	0.005 ± 0.001
N	1st and 2nd	14.0 ± 0.1	13.9 ± 0.3	13.7 ± 0.4	13.6 ± 0.3
$N_{Cu,Ni}$		1 ± 2	2 ± 2	1 ± 2	1 ± 2

Therefore, these observations have to be interpreted in terms of an accumulation of Cu in the atomic environment of Cu-atoms, i.e. a formation of small Cu-clusters despite its lower concentration in the RPV-steel. Thus, most of the $N_{Cu,Ni}$ around Cu seems to be Cu, while the opposite is true for Ni, i.e. the local environment of Ni is mainly formed by Ni and not by Cu. This is consistent with the more or less constant value of $N_{Cu,Ni}$ determined from the experiments at the Ni K-edge. This is a quite surprising result since the concentration of Ni in the RPV-steel matrix is about 11 times higher compared to Cu. The Cu atoms seem to exhibit an extremely high mobility in the steel lattice, and in parallel, they seem to pin each other, leading to nano-sized precipitates even during the early stages of neutron irradiation. This underlines the prominent role of copper observed in the embrittlement of RPV steels [9,10].

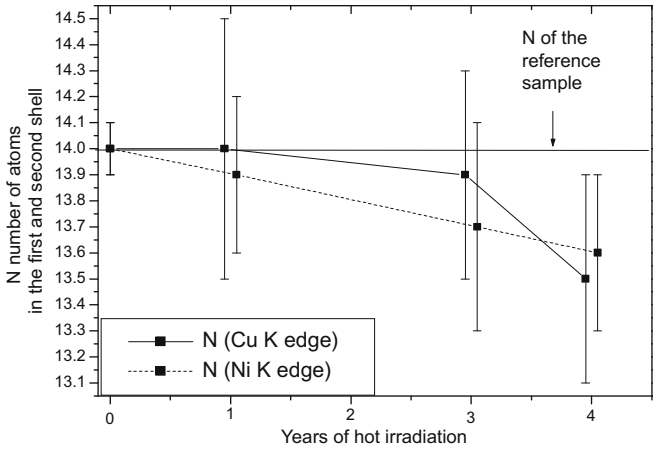

Fig. 7. Number of atoms in the first and second shell of the absorbers at the Cu and Ni K-edge. Note that the years of irradiation are slightly shifted to avoid annoying overlap.

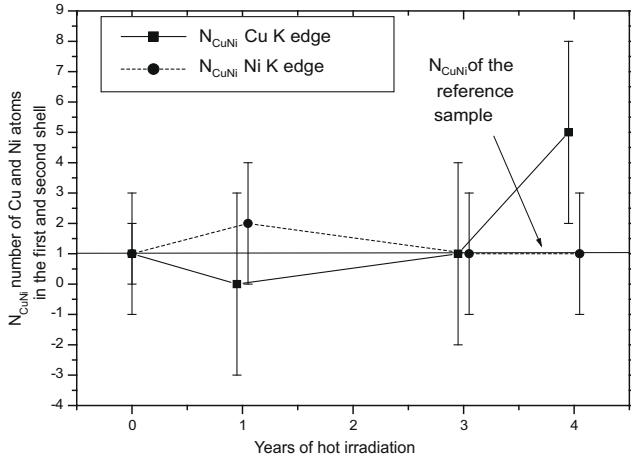

Fig. 8. Number of the atoms of Cu and Ni in the first and second shell around the absorber at the Cu and Ni K-edge. Note that the years of irradiation are slightly shifted to avoid annoying overlap.

5. Conclusions

Three RPV surveillance samples, irradiated in the nuclear power plant of Gösgen (Switzerland), as well as unirradiated reference material have been analyzed by EXAFS at the Cu and Ni K-edges. Although RPV steels have a complex composition, it could be shown that EXAFS can be applied to investigate Cu clusters providing quantitative data within the first and the second shells. Both Cu and Ni atoms reside in a bcc environment, similar to the Fe matrix. Neutron irradiation in the reactor at 575 K did not induce any major lattice type changes under the given conditions. However, neutron irradiation in reactor leads to small changes of the local atomic environment around the investigated Cu and Ni atoms, since a slight reduction of the number of next neighbours in the bcc-structure around Cu and Ni in the steel matrix was observed. This reduction is likely to be proportional to the number of years of irradiation in reactor, and thus, most of the local structural changes are obtained for the sample with the longest irradiation time. It can be expected that the elevated temperature of the reactor partially helps the refilling of the irradiation induced vacancies by a kind of annealing processes. The detailed EXAFS analysis has demonstrated that the number of Cu atoms in the local vicinity of copper is enriched during irradiation at elevated temperature, while the local atomic environment around nickel seems to be more or less unaffected. This different behaviour between Cu and Ni absorbers has never been observed earlier.

Acknowledgments

Thanks go to the micro-XAS scientists at the SLS, PSI, and the XAFS beamline scientists at ANKA, FZK, for the precious technical support and to R. Knobel from Kernkraftwerk Gösgen for the valuable detail information about the sample material. The sample preparation was done by A. Bullemer, PSI.

References

[1] M.K. Miller, M.G. Burke, J. Nucl. Mater. 195 (1992) 68.
[2] P. Pareige, M.K. Miller, Appl. Surf. Sci. 94&95 (1996) 370.
[3] K. Fukuya, K. Ohno, H. Nakata, S. Dumbill, J.M. Hyde, J. Nucl. Mater. 312 (2003) 163.
[4] P. Pareige, B. Radiguet, A. Suvorov, M. Kozodaev, E. Krasicov, O. Zabusov, J.P. Massoud, Surf. Interf. Anal. 36 (2004) 581.
[5] M.K. Miller, M.A. Sokolov, R.K. Nanstad, K.F. Russel, J. Nucl. Mater. 351 (2006) 216.
[6] Y. Nagai, Z. Tang, M. Hassegawa, T. Kanai, M. Saneyasu, Phys. Rev. B 63 (2001) 134110.
[7] R.G. Carter, N. Soneda, K. Dohi, J.M. Hyde, C.A. English, W.L. Server, J. Nucl. Mater. 298 (2001) 211.

[8] M.K. Miller, K.F. Russel, M.A. Sokolov, R.K. Nanstad, J. Nucl. Mater. 320 (2003) 177.
[9] B. Radiguet, A. Barbu, P. Pareige, J. Nucl. Mater. 360 (2007) 104.
[10] G. Kuri, C. Degueldre, J. Bertsch, J. Rothe, J. Nucl. Mater. 362 (2007) 274.
[11] F. Maury, N. Lorenzelli, M.H. Mathon, C.H. de Novion, P. Lagarde, J. Phys.: Condens. Mater. 6 (1994) 569.
[12] A.B. Edwards, K.J. Roberts, S. Pizzini, W. Phythian, Phil. Mag. A 79 (6) (1999) 1295.
[13] P. Pareige, B. Radiguet, A. Barbu, J. Nucl. Mater. 352 (2006) 75.
[14] M.K. Miller, B.D. Wirth, G.R. Odette, Mater. Sci. Eng. A 353 (2003) 133.
[15] P. Pareige, R.E. Stoller, K.F. Russel, M.K. Miller, J. Nucl. Mater. 249 (1997) 165.
[16] P. Auger, P. Pareige, S. Welzel, J.-C. Van Duysen, J. Nucl. Mater. 280 (2000) 331.
[17] M.K. Miller, K.F. Russel, P. Pareige, M.J. Starink, R.C. Thomson, Mater. Sci. Eng. A 250 (1998) 49.
[18] G. Salje, M. Feller-Kniepmeier, J. Appl. Phys. 48 (2006) 1833.
[19] P.A. Lee, P.H. Citrin, P. Eisenberger, B.M. Kincaid, Rev. Modern Phys. 53 (1981) 769.
[20] J.J. Rehr, R.C. Albers, Rev. Modern Phys. 72&73 (2000) 621.
[21] D. Grolimund, M. Senn, M. Trottmann, M. Janoush, I. Bonhoure, A.M. Scheidegger, M. Marcus, Spectrochim. Acta 59 (2004) 1627.
[22] C. Degueldre, K. Dardenne, Nucl. Instrum. Meth. B 238 (2005) 323.
[23] M. Newville, J. Synchrotron Rad. 8 (2001) 322.
[24] B. Ravel, M. Newville, J. Synchrotron Rad. 12 (2005) 537.
[25] B. Ravel, J. Synchrotron Rad. 8 (2001) 314.